Applied Catalysis B: Environmental 176–177 (2015) 288–297

Contents lists available at ScienceDirect

Applied Catalysis B: Environmental

journal homepage: www.elsevier.com/locate/apcatb

Effect of surfactant concentration on active species generation and photocatalytic properties of TiO_2

Ekemena Oghenovoh Oseghe, Suresh Maddila, Patrick Gathura Ndungu, Sreekanth Babu Jonnalagadda*

School of Chemistry and Physics, University of Kwa-Zulu Natal, Westville Campus, Private Bag X 54001, Durban 4000, South Africa

ARTICLE INFO

Article history:
Received 8 December 2014
Received in revised form 30 March 2015
Accepted 6 April 2015
Available online 8 April 2015

Keywords:
Surfactant concentration
TiO_2 nanoparticle
Photocatalysis
Hydroxyl radical
Oxygen vacancy

ABSTRACT

The importance of varying surfactant concentration in TiO_2 synthesis and its effect on the formation of OH radical, oxygen vacancy, and photocatalytic properties is the focus of this work. The sol–gel method was adopted in the synthesis of TiO_2 nanoparticles and calcined in air/argon at 400 °C. In a typical synthesis, the concentration of non-ionic surfactant, pluronic F127, was varied by mass relative to the concentration of TiO_2 precursor. The as-prepared materials were characterized by X-ray powder diffraction (XRD), scanning electron microscopy (SEM), high resolution transmission electron microscopy (HRTEM), N_2 sorption, Raman spectroscopy, fluorescence spectrometry, and electron spin resonance spectroscopy (ESR). Photocatalytic properties of the materials were evaluated by monitoring the decoloration of 10 mg/L model dye, methylene blue at pH 3, 7, and 11 in the presence of different light sources. Pore size distribution calculated from the Barrett–Joyner–Halenda (BJH) shows that the materials are both meso- and macroporous with surface area of 48–110 cm^2/g. The as-prepared TiO_2 nanoparticles existed in the anatase phase with a decrease in crystal size as the concentration of the surfactant used in synthesis increased. An increase in OH radical and surface oxygen vacancy formation was also observed as the concentration of surfactant used in synthesis increased. The as-prepared TiO_2, calcined in air and argon, T_1:S_3AA, showed the best photocatalytic activity resulting from its relatively higher hydroxyl radical generated and surface oxygen vacancy.

1. Introduction

A number of semi-conductors of high quality have been extensively studied in order to develop a more efficient photocatalytic system. TiO_2 has proven to be one of the best semi-conductors for this process. This is because it is stable; most efficient; cheap and environmentally benign. The photocatalytic mechanism for the decoloration of model dyes by TiO_2 has been classified into direct and indirect pathway [1]. OH radical and photogenerated holes are key species needed by the two mechanisms for photodecoloration of dyes. The direct mechanism is based on the photo-induced generation of electrons and holes by the catalyst. The photo-generated hole is then trapped by either the adsorbed dye on the surface of the catalyst or surface defects to form reactive radicals or surface active centers, respectively. The adduct species formed when dyes reacts with either the holes or surface active centers, would either decompose or recombine with electrons to form intermediates and products [2,3]. In the indirect mechanism, OH radical is formed when the photogenerated electron and holes reacts with adsorbed water and O_2. The generated OH radical is responsible for the decoloration of the dye forming intermediates and products [4]. Some other factors considered influential in improving the photocatalytic properties of TiO_2 are particle size, specific surface area, crystal structure and size [5,6].

Several efforts have been made to synthesize TiO_2 with good photocatalytic properties by changing variables during preparations. Some of these variables include solvent variation [5], pH of the reaction media [7], calcination temperatures [8,9], dopant concentration [10–12], surfactant [13] and surfactant concentration [14]. Xiao et al. [15] observed an enhanced photocatalytic degradation of methylene blue under UV irradiation resulting from high specific surface area and increased formation rate of hydroxyl radical by Sm^{3+} doped TiO_2. Tryba et al. [8] also showed a relationship between crystallinity stemming from heat treatment temperature and the formation rate of OH radical.

* Corresponding author. Tel.: +27 31 2607325; fax: +27 31 2603091.
E-mail address: jonnalagaddas@ukzn.ac.za (S.B. Jonnalagadda).

http://dx.doi.org/10.1016/j.apcatb.2015.04.010
0926-3373/

TiO_2 nanoparticles can either be synthesized with or without templates [16]. When synthesized by a template-based method, there are various options available such as soft (surfactants and block polymers) or hard templates – porous silica, polysterene spheres, and porous carbon. For the soft template, the synthesis of mesoporous materials significantly depends on surfactant micelles and liquid crystals acting as structure directing agents [17]. The effect of surfactant concentration on film thickness and efficiency of dye-sensitized solar cells, particle sizes and morphology of TiO_2 has been studied [14,18]. To the best of our knowledge, there are no studies on the effect of surfactant concentration investigated in the synthesis of TiO_2 on its rate of OH radical formation consequently.

In this work, we report on the synthesis of mesoporous TiO_2 with different concentrations of non-ionic surfactant, pluronic F127, as structure directing agent. The effect of varying pluronic F127 concentration and calcination conditions on oxygen vacancy, OH radical generation, and photocatalytic decoloration of methylene blue (MB) by the as-prepared TiO_2 were also discussed.

2. Materials and methods

Sol–gel technique, which has been applied in the synthesis of several nanomaterials [19–21] is adapted in the synthesis of TiO_2. Titanium (IV) isopropoxide (TIP), purchased from Sigma–Aldrich (MW = 284.22, 97%) was used as TiO_2 precursor. The solvent used consisted of a mixture of 1-propanol (Sigma–Aldrich, HPLC grade) and ultra-pure water (1:2.5 by volume), and a non-ionic surfactant, Pluronic F-127 (Sigma–Aldrich), as the structure directing agent. The schematic representation of the synthesis of TiO_2 is presented in Scheme 1. In a typical synthesis of the various samples, 50 mL of ultra-pure water of pH 11 (adjusted with 0.1 M HNO_3 or 0.1 M NaOH) was measured into a 600 mL Pyrex beaker and placed under stirring. Surfactant masses of 2.5, 5, 10, and 15 g were dissolved in 10 mL of 1-propanol, added to the pH adjusted water and allowed to stir for 10 min. Five gram of the (TIP) was mixed with 10 mL of 1-propanol, and then added slowly drop by drop to the surfactant solvent mixture. After approximately 4.0 h, the stirring was stopped and aged for 24 h at room temperature and for another 24 h at about 80 °C. The samples after aging were placed in an alumina

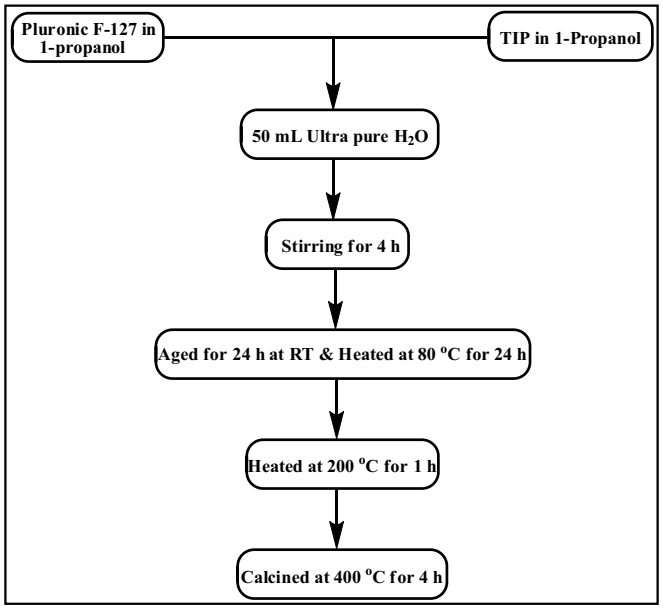

Scheme 1. Schematic illustration of the synthesis procedure of TiO_2.

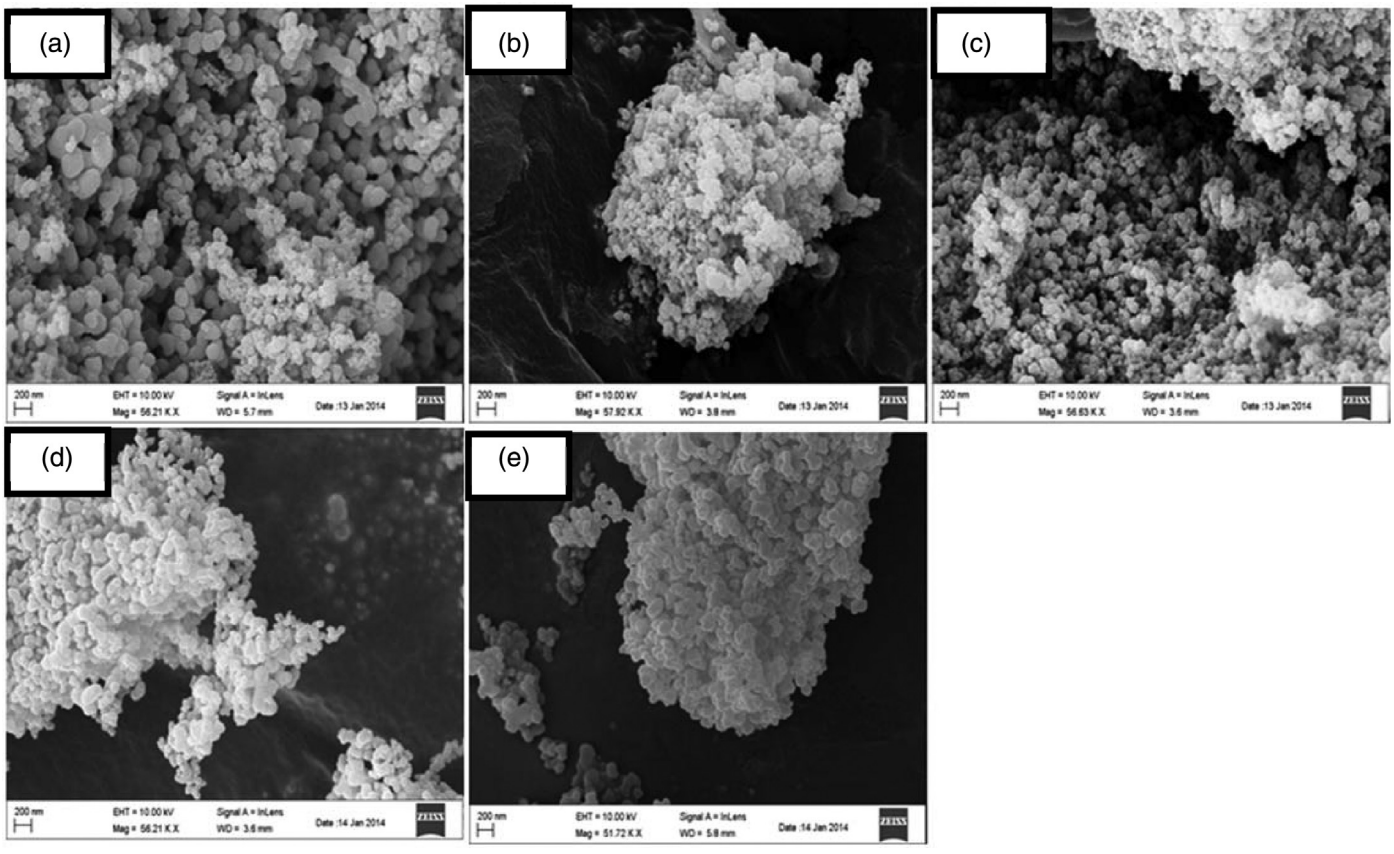

Fig. 1. SEM micrographs of (a) T_2:S_1, (b) T_1:S_1, (c) T_1:S_2, (d) T_1:S_3, and (e) T_1:S_3AA.

boat and transferred to a horizontally aligned tube furnace. Samples were then heat treated at 200 °C for 1 h, and ramped at the rate of 2 °C/min to 400 °C for 4 h. The resulting samples were marked as T_2:S_1, T_1:S_1, T_1:S_2, T_1:S_3, where T = titanium, S = surfactant and the subscripts represents the ratio of titania precursor to surfactants by mass. An optimized sample was synthesized by changing the calcination condition of T_1:S_3 – heat treated in argon at 200 °C for 1 h, increased to 400 °C for 2 h and finally calcined at 400 °C for 8 h in air (ramp rate was 2 °C/min). The resulting sample was marked T_1:S_3AA, where AA represents the calcination environment (argon and air).

2.1. Catalyst characterization

The surface morphology of the materials was examined on a scanning electron microscope (ZEISS Ultra /Plus FEG-SEM). Detailed physical structural characteristics were observed with a JEOL JEM-1010 high resolution transmission electron microscope (HRTEM). The phases of the materials were observed using powder X-ray diffraction (XRD) conducted on a Bruker D8 advance instrument, equipped with a XRK 900 reaction chamber, a TCU 750 temperature control unit and a Cu Kα radiation (λ = 0.15406 nm). The textural characteristics were determined by using a Micrometrics Tri-Star II 3030 instrument. Samples were degassed prior to textural analysis by using a Micrometrics Flow Prep (060) under N_2 flow at 90 °C for 1 h, and then increasing the temperature to 200 °C, and leaving the samples to de-gas for approximately 12 h. UV–vis diffuse reflectance spectra were recorded with an Ocean Optics high resolution spectrometer (HR2000+) equipped with a halogen light source (HL-2000-FHSA) and an integrating sphere accessory, using $BaSO_4$ as a reference. Infrared spectra of the samples were recorded using Fourier transmission infrared (FTIR) spectrometer (PerkinElmer spectrum 100 series with universal ATR accessory). Photoluminescence spectroscopic study of the materials was performed on a PerkinElmer LS 55 fluorescence spectrophotometer, where the samples were excited with higher photon energy (310 nm). EPR data was collected at room temperature on a microwave resonator of a Bruker EMX-plus X-band ESR spectrometer. Data acquisition: frequency, 9.853713 GHz; power, 2.00 mW; modulation amplitude, 2.00 G (modulation frequency 100.00 kHz); time constant, 81.92 ms; conversion time, 18.00 ms; sweep width, 2500 G (centre field = 3500 G); data resolution, 5000 points.

2.2. Hydroxyl radical generation and photocatalytic tests

Dosimetry method was used to determine the OH radical formation. In a typical procedure, 250 mg/L of the catalyst was added to 200 mL of the 0.1 mM terephthalic acid (TA) solution in 2 mM NaOH, and was then irradiated with a 32 W daylight compact fluorescent lamp (CFL). Sampling was performed at every 20 min interval. Solution after centrifuging at 14000 r/min was analyzed on a PerkinElmer LS 55 fluorescence spectrophotometer. The product of terephthalic acid hydroxylation, 2-hydroxyterephthalic acid (2-HTA), gave a peak at the wavelength of about 425 nm when excited at 310 nm. This procedure was repeated using 100 mg/L of catalyst with a 32 W daylight CFL and a 300 W halogen lamp. Photodegradation studies of methylene blue (MB) were carried out in a simple quartz photochemical reactor day light lamp. Prior to light irradiation, 250 mg/L of photocatalyst was added to 200 mL

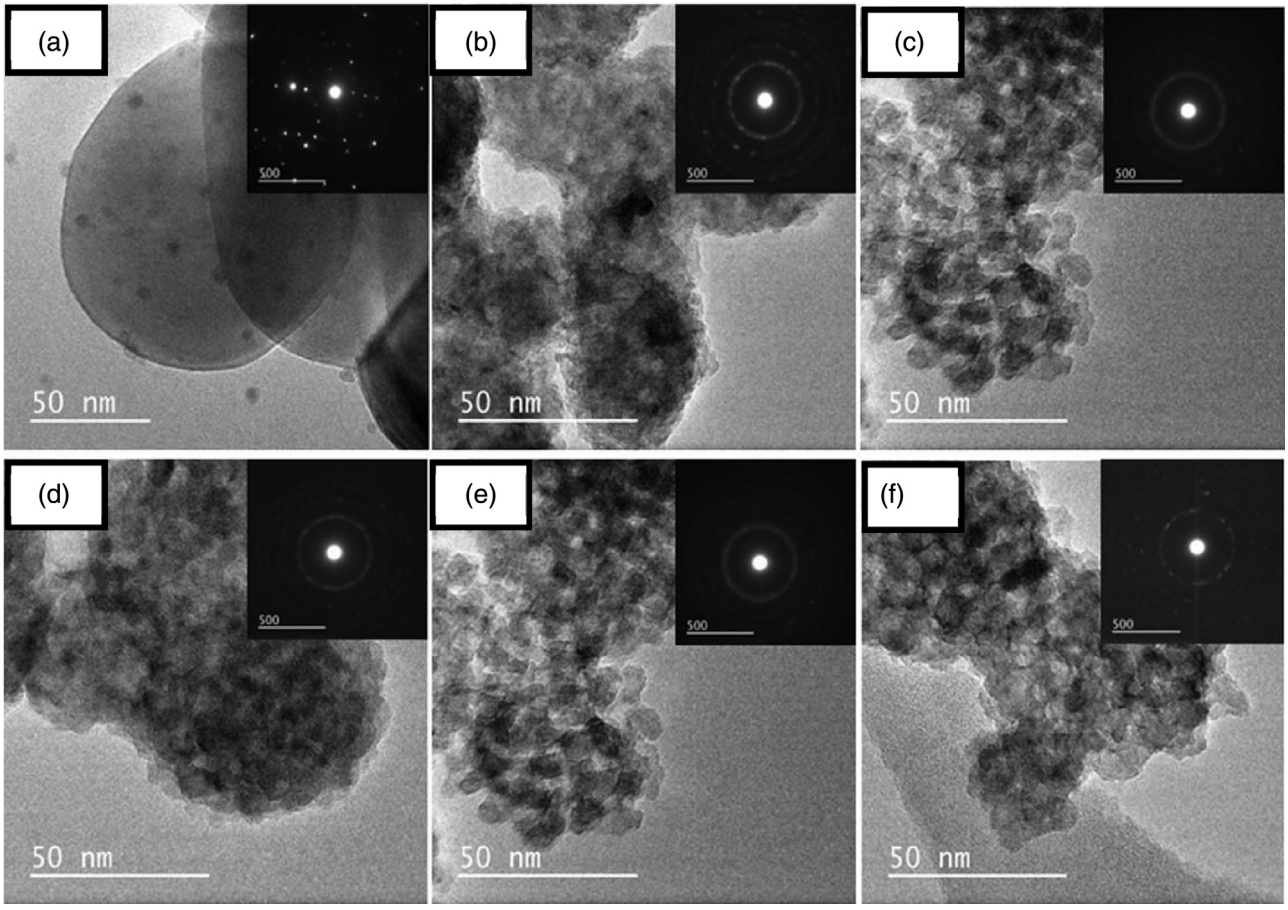

Fig. 2. HRTEM micrographs and diffraction patterns (insert) of (a) Commercial TiO_2, (b) T_2:S_1, (c) T_1:S_1, (d) T_1:S_2, (e) T_1:S_3, and (f) T_1:S_3AA.

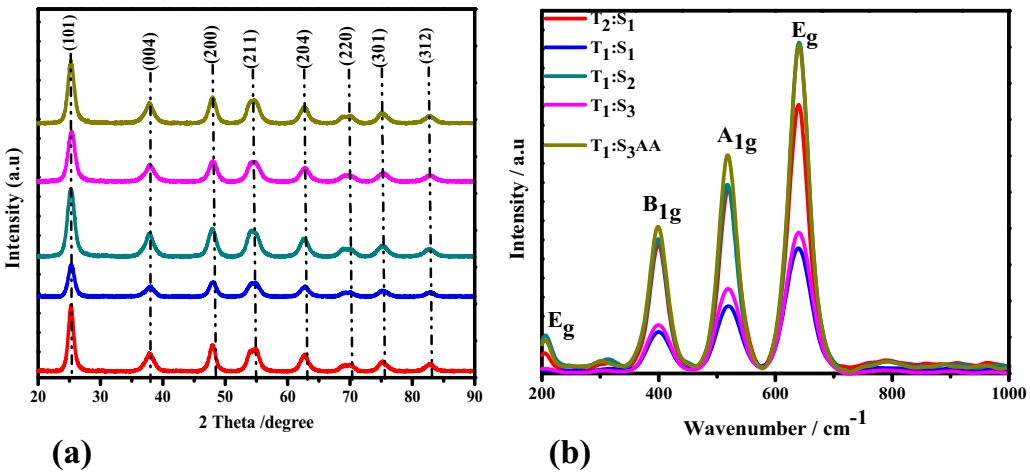

Fig. 3. X-ray diffractogram (a) and Raman spectra (b) of T_2:S_1 (red), T_1:S_1 (blue), T_1:S_2 (dark cyan) T_1:S_3 (pink), and T_1:S_3AA (dark yellow). (For interpretation of the references to color in this figure legend, the reader is referred to the web version of this article.)

of MB (10 mg/L) aqueous solution of pH 11, and the mixture was first sonicated for 10 min and then stirred in the dark for 1 h to attain adsorption–desorption equilibrium. The light source was a 32 W daylight CFL (solar power = 1.72 W/m^2, UV = 2.25 W/m^2, λ = 300–1000 nm as measured by solar irradiance meter (TM-208) and Ocean Optics high resolution spectrometer (HR2000+). At given time intervals (20 min), aliquots (2 mL) were taken from the solution and immediately centrifuged at 14000 r/min for 5 min, and the absorbance taken on a UV–vis spectrometer (Libra S6) at 665 nm. The measured absorbance was converted to concentration by using a calibration curve constructed from known concentrations of MB. This same procedure was repeated using 100 mg/L of catalyst in a 200 mL MB solution (10 mg/L) of pH 11, 7 and 3 under a 300 W halogen lamp (solar power = 585 W/m^2, UV = 0.82 W/m^2, λ = 342–1000 nm as measured by solar irradiance meter (TM-208) and Ocean Optics high resolution spectrometer (HR2000+)).

3. Results and discussion

3.1. Morphology

Fig. 1a–e shows the SEM micrographs of the as-prepared materials. The materials comprised both agglomerated and aggregated particles of spherical and irregular shape, possessing size ranging from 50 to 180 nm with interparticle voids. HRTEM micrographs (Fig. 2a–f) confirms the particles are more of agglomerates and aggregates than dispersed. The commercial TiO_2 possesses large individual particles averaging 146 nm in size with smaller particles, 5 nm, dispersed on each individual particle. The selected area electron diffraction pattern (SAED), inserts of Fig. 2a–f, shows the polycrystalline characteristics of the materials. Among the as-prepared materials, T_2:S_1 exhibited relatively higher crystallinity. TiO_2 calcined in both air and argon, T_1:S_3AA showed better crystallinity than its counterpart, T_1:S_3, calicined in air. This might be due to the duration of calcination which could favor crystal growth.

3.2. Crystalline structure

The crystal phase and sizes are some important characteristics of a good photocatalyst [6]. These characteristics were investigated in the materials using the XRD. Fig. 3a shows the XRD diffraction pattern of the materials. As-prepared materials exist in the anatase phase as confirmed from the JCPDS file no. 21-1272, and showed relatively broader peaks than the commercial material. The characteristic broad peaks of the materials are distinctive for polycrystalline/nanosized materials. Scherrer's equation was used in estimating the crystal size (D) of the materials and the results are shown in Table 1.

$$D = \frac{K\lambda}{\beta \cos\theta}$$

where K is a constant (≈0.9), λ is the X-ray wavelength, 0.15418 nm, β is the full width at half maximum (FWHM) of the diffraction peak, and θ is the diffraction angle. The values of β and θ are taken from the crystal plane (1 0 1) of the materials. The crystallinity (FWHM) and crystal size of the synthesized TiO_2 decreased from 7.84 to 6.11 nm with increase in surfactant concentration. This implies an increased surfactant concentration inhibits anatase grain growth. The anatase grain growth was favored upon calcining in air and argon (T_1:S_3AA) as its crystal size was higher than TiO_2 calcined in air alone. This result corroborates results obtained from the SAED (insert of Fig. 2). Raman analysis was also carried out to confirm

Table 1
Summary of the textural characterizations and XRD analysis on the various as-prepared materials.

Samples	BET surface area (cm^2/g)	Pore volume (cm^3/g)	Pore diameter (nm)	Particle size (nm)	FWHM (101)	Anatase crystal size (101) (nm)	Lattice parameter (A°)	Unit cell volume (A°)^3
T_2:S_1	48.36	0.2930	23.42	106.38	0.0181	7.84	$a = b = 3.7956$ $c = 9.4988$	136.85
T_1:S_1	85.54	0.3160	13.07	58.33	0.0202	7.04	$a = b = 3.7922$ $c = 9.4898$	136.47
T_1:S_2	110.00	0.4388	14.17	45.34	0.0231	6.17	$a = b = 3.7979$ $c = 9.5079$	137.14
T_1:S_3	73.23	0.2521	13.30	47.42	0.0233	6.11	$a = b = 3.7910$ $c = 9.4898$	136.38
T_1:S_3AA	70.11	0.2607	14.05	50.18	0.0203	7.01	$a = b = 3.7956$ $c = 9.5124$	137.04

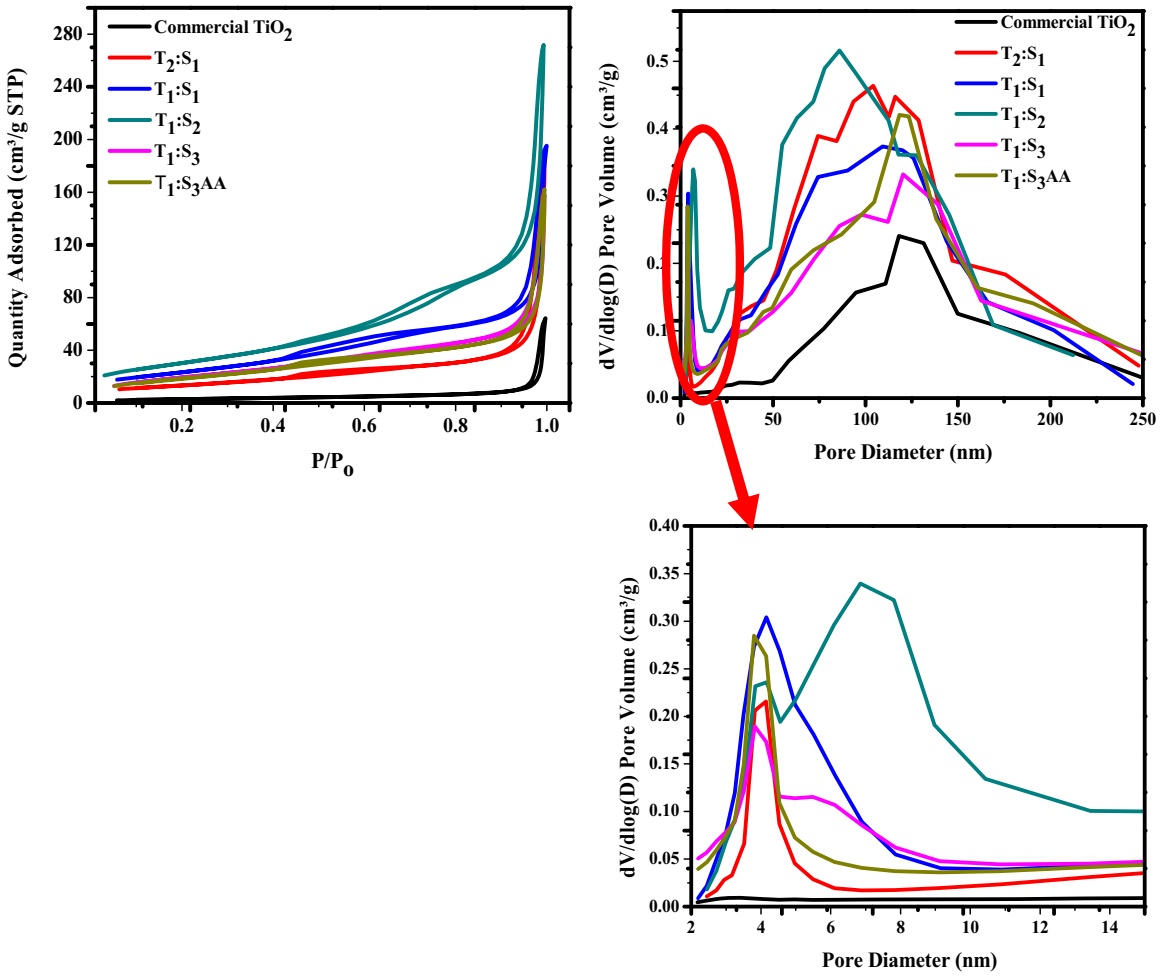

Fig. 4. N_2 sorption isotherm (a), BJH pore size distribution (b and c) of the materials.

the crystal phase of the materials. As shown in Fig. 3b, as-prepared materials possess well-defined vibrational bands at 197, 396, 516 and 639 cm^{-1}. These bands corresponds to the E_g, B_{1g}, A_{1g} and E_g bands, respectively, which are typical for the anatase phase [10,22,23].

3.3. Textural properties

N_2 sorption of the materials was carried out to measure their textural properties. Fig. 4 shows the N_2 sorption isotherm and BJH desorption pore size distribution curve of the materials. The sorption isotherms of the as-prepared materials are typical for type IV with dual H1 hysteresis loops appearing at 0.4–0.8 P/Po, and 0.9 P/Po [24]. This suggests the particle size of the as-prepared materials are distributed in both mesoporous and macroporous region (Fig. 4b and c). The macroporous characteristic of the as-prepared materials might be due to interparticle voids [25]. The sorption isotherm of the commercial TiO_2 showed it is non-porous with its macropores resulting from interparticle voids [25]. The BET surface area, BJH pore volume, BJH pore diameter and particle size are summarized in Table 1. The particle size of the as-prepared materials decreased as the surfactant concentration increased with T_1:S_2 having the smallest particle size and the highest surface area. A decreased surface area exhibited by T_1:S_3 and T_1:S_3AA might be due to structural collapse resulting from excess surfactant concentration and heat treatment [26–28].

Table 2
Assignment of signal obtained from the EPR spectra.

Samples	*G* factor
Commercial TiO_2	1.9941 1.9708 1.9424
T_2:S_1	1.9985
T_1:S_1	2.0021
T_1:S_2 T_1:S_3	2.0679 2.01252.0729 1.9993
T_1:S_3AA	2.0872 1.9993

Table 3
Effect of light source on the formation rate of OH radical.

Light source	Commercial TiO_2		T_1:S_3AA	
	K_{OH}	R^2	K_{OH}	R^2
32 W Daylight CFL	4.0713×10^{-5}	0.9650	2.4054×10^{-5}	0.9888
300 W Halogen lamp	4.0206×10^{-5}	0.9854	1.1710×10^{-5}	0.9930

3.4. Electron spin resonance

ESR was the instrument used for identifying signals resulting from paramagnetic species [29]. The characteristic ESR spectra for the as-prepared and commercial TiO_2 are presented in Fig. 5. The spectra show the materials generate paramagnetic signals with their characteristics *g*-values (Table 2). All as-prepared TiO_2 except T_2:S_1 exhibited *g*-values greater than 2 which could be ascribed to the formation of hole trapping sites [30,31]. A gradual shift of the *g*-values and decrease/disappearance of the hole trapping signals was observed as the concentration of the surfactant decreased.

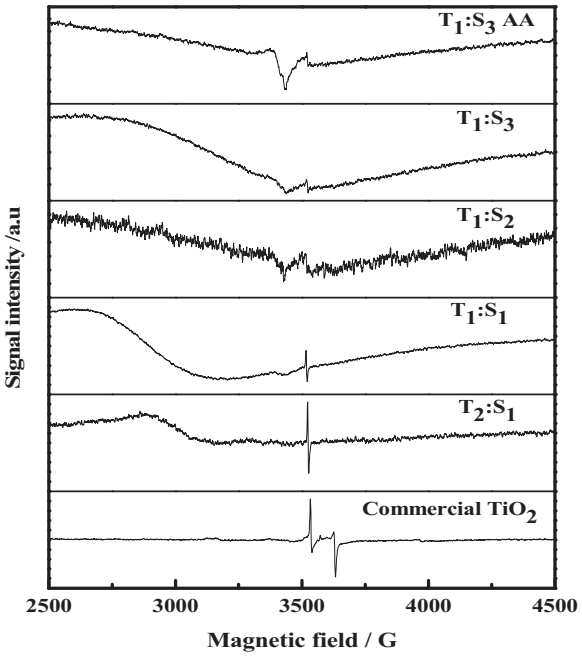

Fig. 5. EPR spectra of the materials.

Materials, T_2:S_1, T_1:S_3, and T_1:S_3AA with $g_\perp$ = 1.9985, 1.9993, and 1.9993 could be assigned to electron trapping sites on the surface of the materials [30]. No hole trapping signal was detected with the commercial TiO_2 but possesses signals typical for electron trapping site, Ti^{3+} [32].

3.5. OH radical generation and photocatalytic properties of the materials

Hydroxyl radical due to its oxidation potential and non-specific characteristic is desired in the oxidation of organic pollutants [33]. The rate of OH radical formation in a photcatalytic system could be determined by the pH of the solution and the phase structure of the material [34]. In order to evaluate the OH radical generation efficiency of the materials, terephthalic acid was used as scavenger. Where the OH radical formed by the materials upon irradiation reacts with terephthalic acid to form highly fluorescent 2-hydroxylterephthalic acid [15].

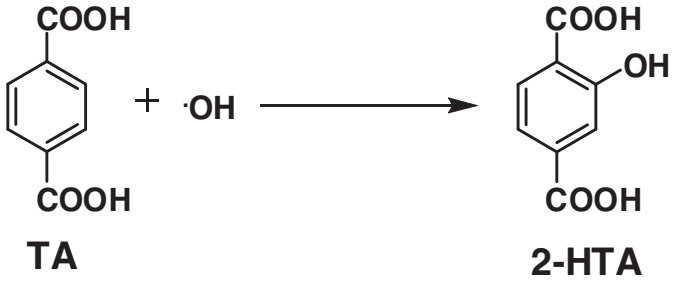

Fig. 6 shows the amount of OH radical generated by the materials upon irradiating with a 32 W daylight CFL. A linear increase in the amount of OH radical generated with irradiation time was observed for all materials, obeying zero order reaction rate kinetics [35]. The formation rates of OH radical by the as-prepared TiO_2 obtained from the slope of Fig. 6a were plotted against each of the as-prepared TiO_2. OH radical formation is directly proportional to the concentration of surfactant used in preparing the materials (Fig. 6b). It is interesting to observe an increase in OH radical formation with the increase in concentration of surfactant used in the synthesis of TiO_2.

The result also shows that as-prepared TiO_2 calcined in argon and air, T_1:S_3AA generated more OH radical than the ones calcined in air alone. Commercial TiO_2 generated more OH radical which could be attributed to its characteristic mixed phase and electron trapping sites [8]. Effect of decreasing catalyst concentration on OH radical generation irradiated with a 32 W daylight CFL was evaluated on commercial TiO_2 and the optimized TiO_2, T_1:S_3AA (Fig. 7a). Commercial TiO_2 showed a decreased formation rate of OH radical from 5.7899×10^{-5} to 4.0713×10^{-5} corresponding to catalyst concentration of 250 mg/L and 100 mg/L, respectively. No obvious change in the formation rate of OH radical was noticed with varying the concentration of T_1:S_3AA. Fig. 7b shows the effect of light sources on the formation of OH radical by the commercial and as-prepared TiO_2. Both materials showed slight decrease in OH radical formation rate with the 300 W halogen lamp, as shown in Table 3. This may result from the relatively higher UV, 2.25 W/m^2 of the 32 W CFL compared with 300 W halogen lamp of UV = 0.82 W/m^2, as measured by solar irradiance meter (TM-208) [4].

The photocatalytic properties of the materials were tested on 10 mg/L MB solution of pH 11 under a 32 W daylight CFL and the result is presented in Fig. 8. All as-prepared materials showed good adsorptive characteristics compared with the commercial TiO_2 in the absence of light (Fig. 8a). The adsorption properties exhibited by the as-prepared materials could be due to their relatively large surface area presented in Table 1 [36]. Among the as-prepared

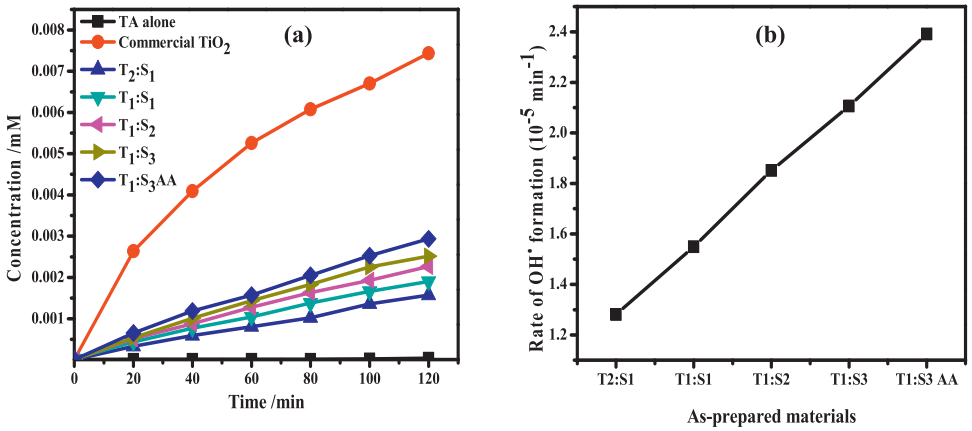

Fig. 6. OH radical generation by (a) 250 mg/L of catalysts in 200 mL, 0.1 mM terephthalic acid solution irradiated with 32 W daylight CFL (b) effect of surfactant concentration on the rate of OH radical formation.

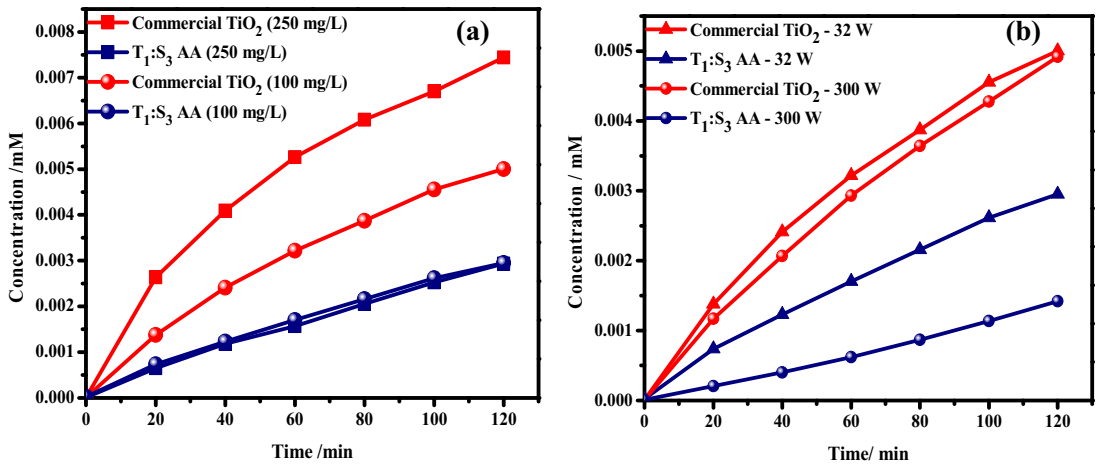

Fig. 7. Effect of catalyst concentration (a) and light source (b) on OH radical formation.

materials, T_1:S_2 with a specific surface area of 110.00 m^2/g had the highest percentage adsorption while T_2:S_1, 48.36 m^2/g, had the least percentage adsorption.

Fig. 8b shows the effect of photons on further removal and decoloration of the MB solution in the presence and absence of photocatalyst. Within 2 h of the reaction, all as-prepared TiO_2 except T_1:S_1 showed better photocatalytic activities than the commercial TiO_2. The optimized as-prepared TiO_2, T_1:S_3AA exhibited the highest photocatalytic efficiency of 42.88% while T_1:S_1 showed the least efficiency of 24.11%. The kinetics for the photocatalytic efficiency of the catalysts is presented in Fig. 8c with plots following the pseudo first-order kinetics. The apparent rate constant, K_{MB} of the catalysts obtained from the slope of the plots are presented in Table 4. It is interesting to see no correlation between the amount of OH

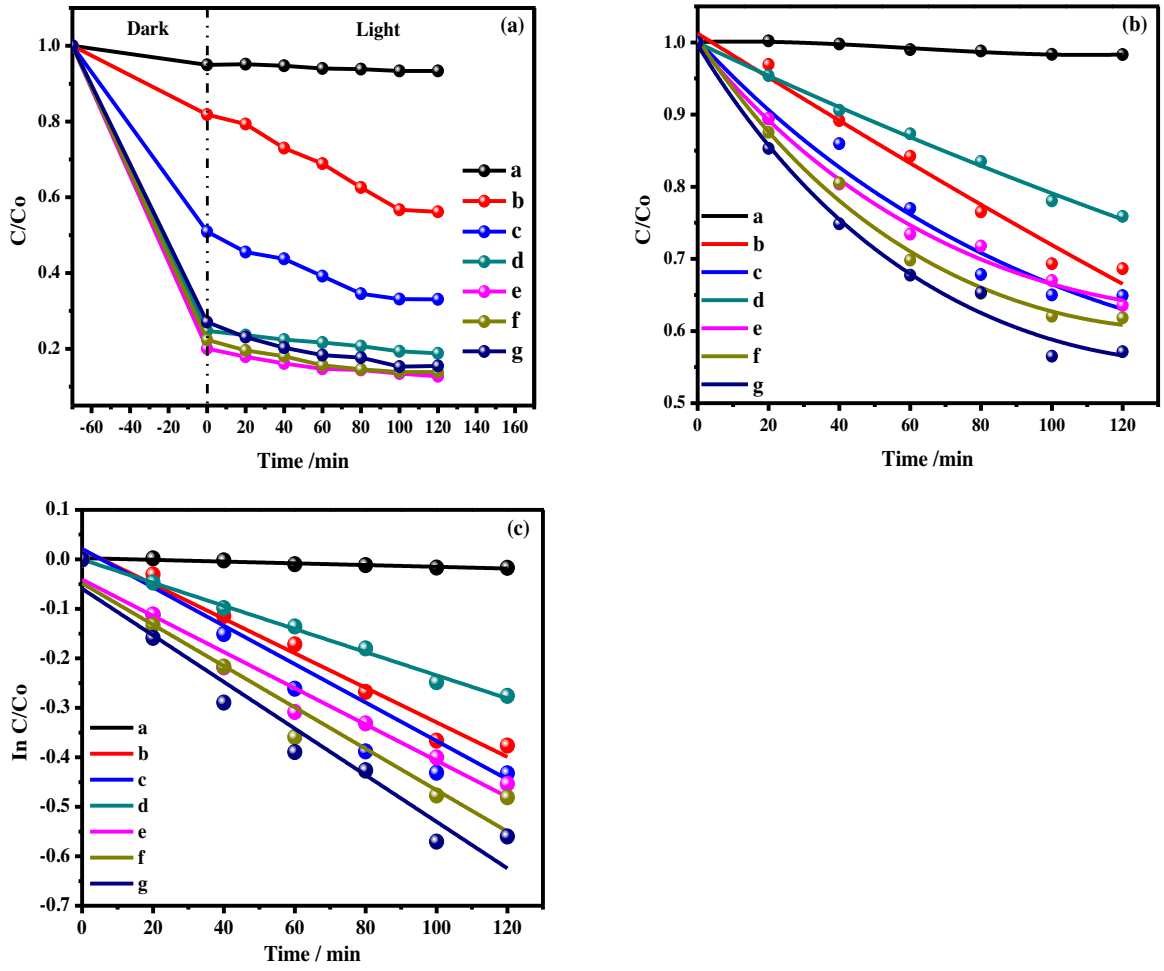

Fig. 8. Adsorption–photodegradation (a) and photocatalytic efficiency (b) of (a) without catalyst, (b) commercial TiO_2, (c) T_2:S_1, (d) T_1:S_1 (e) T_1:S_2, (f) T_1:S_3 (g) T_1:S_3AA irradiated with 32 W daylight CFL.

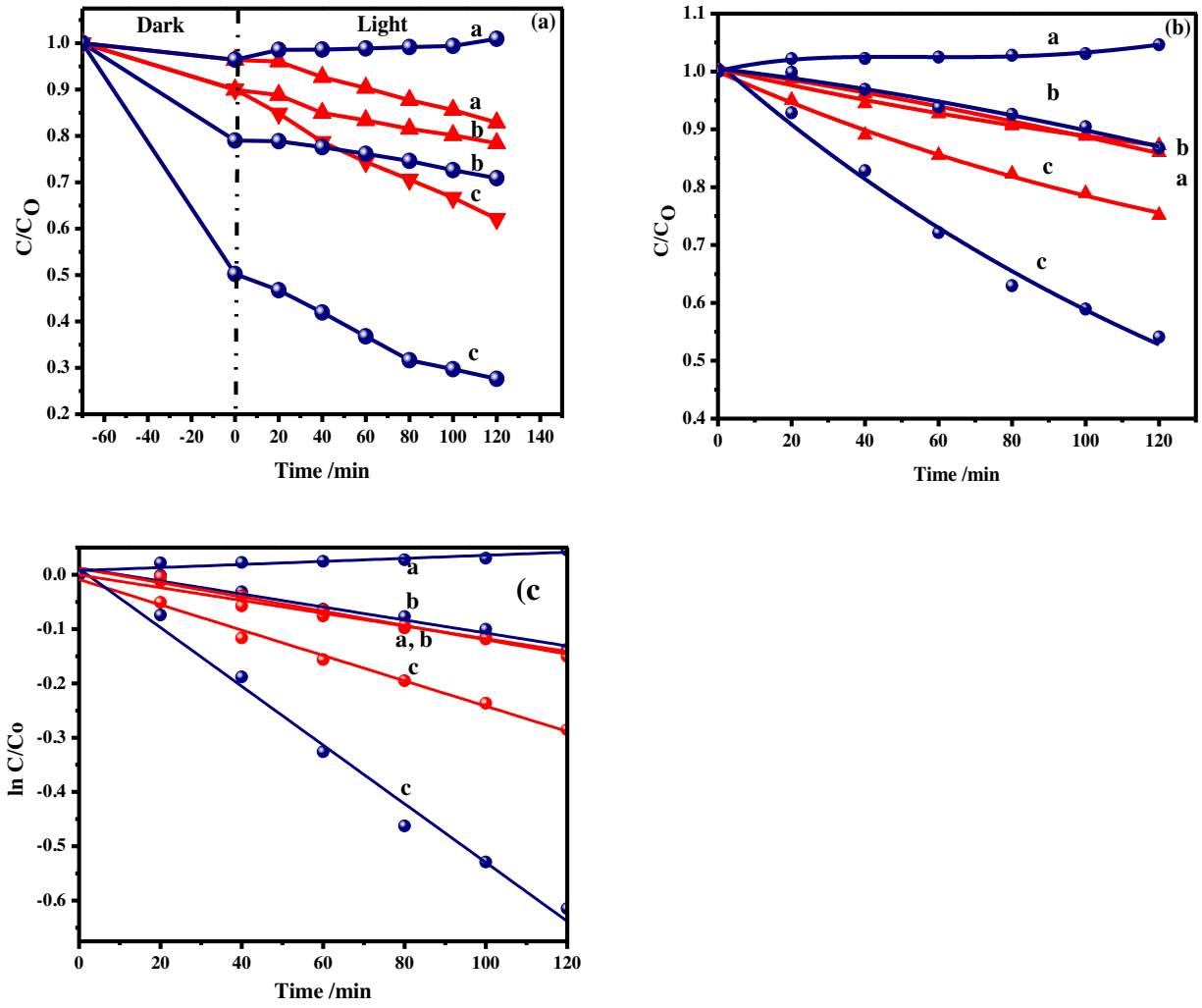

Fig. 9. Adsorption–photodegradation (a); photocatalytic efficiency (b); and pseudo-first order kinetics for commercial TiO_2 (red) and T_1:S_3AA (navy) where a, b, and c corresponds to pH 3, 7, and 11 MB solution, respectively, irradiated with 300 W halogen lamp. (For interpretation of the references to color in this figure legend, the reader is referred to the web version of this article.)

Table 4
Pseudo first order kinetics and adsorption efficiency of the materials.

Sample ID	Rate constant	R^2	Adsorption (%)
Commercial TiO_2	3.49×10^{-3}	0.9735	18.19
T_2:S_1	3.88×10^{-3}	0.9460	49.09
T_1:S_1	2.34×10^{-3}	0.9937	75.25
T_1:S_2	3.66×10^{-3}	0.9559	80.00
T_1:S_3	4.18×10^{-3}	0.9259	77.63
T_1:S_3AA	4.71×10^{-3}	0.9383	72.93

Table 5
Pseudo first order kinetics and adsorption efficiency at different pH media.

Sample ID	Rate constant	R^2	Adsorption (%)
Commercial TiO_2, pH 11	2.33×10^{-3}	0.9923	10.00
Commercial TiO_2, pH 7	1.17×10^{-3}	0.9774	10.00
Commercial TiO_2, pH 3	1.32×10^{-3}	0.9822	3.61
T_1:S_3AA, pH 11	5.41×10^{-3}	0.9880	49.73
T_1:S_3AA, pH 7	1.20×10^{-3}	0.9645	20.96
T_1:S_3AA, pH 3	2.81×10^{-4}	0.7838	3.52

radical generated (Figs.6a and 8b) and the photocatalytic activities of the materials. This implies the photocatalytic mechanism for MB decoloration is not based solely on generated OH radical but via the direct mechanism due to their relatively high surface area and hole trapping sites [1,8].

To confirm the photocatalytic mechanism, T_1:S_3AA with the highest K_{OH} and K_{MB}, and the commercial TiO_2 were applied in MB decoloration at pH 3, 7, 11 under a 300 W halogen lamp irradiation. Fig. 9 shows the adsorption–photodecoloration efficiency of the materials in different pH media. T_1:S_3AA and commercial TiO_2 exhibited better efficiency in the basic (pH 11) media and decreases as it tends toward a lower pH (pH 3) media. Table 5 summarizes the key data from the pH experiments. A decrease in the total MB adsorbed and decolorized by T_1:S_3AA was observed as the pH of the MB solution tends towards acidic region, pH 3. The pH of a solution and the nature of dyes plays vital role on the surface charge and adsorptive properties of the photocatalyst [37,38]. The effect of pH on the adsorption–photodecoloration efficiency of the materials is explained based on the electrostatic interaction between the substrate to be degraded and the surface charge on the photocatalyst. TiO_2 has an isoelectric point (point of zero charge (PZC)) ranging from 6.5 to 6.8 [38–40]. It deprotonates at pH greater than its PZC, hence possessing negatively charged surface which would exert an electrostatic force of attraction towards a positively charged substrate. The reverse is the case when pH of the solution is less than the PZC of TiO_2 [4,37].

$$TiOH + H^+ \rightarrow TiOH_2^+ \quad (1)$$

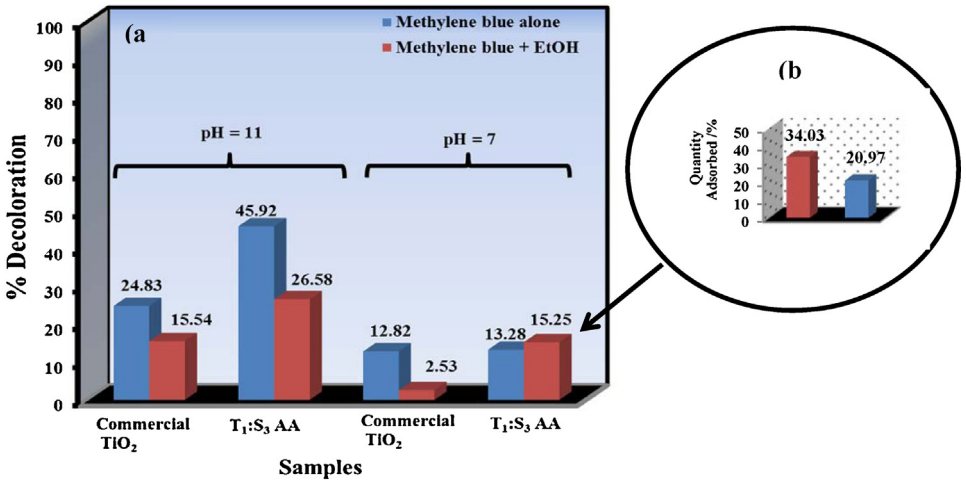

Fig. 10. Effect of scavenging OH radical on MB decoloration at different pH, 11 and 7 (a), quantity of MB adsorbed by T_1:S_3AA in the presence and absence of ethanol at pH 7 (b).

$$TiOH + OH^- \rightarrow TiO^- + H_2O \quad (2)$$

MB being a cationic dye, would therefore be electrostatically attracted to TiO_2 at basic condition (pH 11) and repulsive in acidic media (pH 3). As observed in Fig. 10, T_1:S_3AA showed better decoloration efficiency than the commercial TiO_2 at pH, 11 and 7 but lower efficiency at pH 3. The high efficiency exhibited by T_1:S_3AA at pH 11 and 7 is due to relatively higher surface area, hence a higher adsorptive and photodecolorisation by the active sites and holes, respectively [37,41]. In photocatalytic oxidation of substrates, two mechanisms are suggested, via the direct and indirect route. Scheme 2 shows the proposed schematic illustration of the mechanism for this present work. When photon of higher or equal energy falls on TiO_2, electrons (e^-) are promoted from the valence band to the conduction band leaving vacancy on the valence band (hole (h^+)).

$$TiO_2 + h\nu \rightarrow e^- + h^+ \quad (3)$$

The hole formed reacts with surface adsorbed H_2O and OH to form hydroxyl radical (OH•) which attacks the dye, MB, to produce intermediates and end products.

$$h^+ + H_2O \rightarrow OH^\bullet + H^+ \quad (4)$$

The photogenerated electrons gets trapped by dissolved O_2, to form superoxide radical anion ($O_2^{\bullet -}$) which undergoes series of reactions to form OH• (Eqs. (5)–(8)).

$$O_2 + e^- \rightarrow O_2^{\bullet -} \quad (5)$$

$$O_2^{\bullet -} + H^+ \rightarrow HO_2^\bullet \quad (6)$$

$$2HO_2^\bullet + H_2O_2 + O_2 \quad (7)$$

$$H_2O_2^\bullet \rightarrow 2OH^\bullet \quad (8)$$

The OH• produced then reacts with the dye, MB, to form intermediates and products. All these steps are known as the indirect mechanism and occur in approximately 100 ns [37,38,42]

$$OH^\bullet + \text{dye} \rightarrow \text{products}$$

In the case of direct mechanism, the dye reacts directly with the holes or the surface active sites where the holes are trapped, forming reactive or adduct species. The species formed recombines with the photogenerated electrons to form products (Eq. (9)). This process occurs in about 1 ns [37,38]

$$Dye^+ + e^- \rightarrow \text{products} \quad (9)$$

For further confirmation the proposed mechanism for MB decoloration, OH• was scavenged with ethanol. Alcohols are good

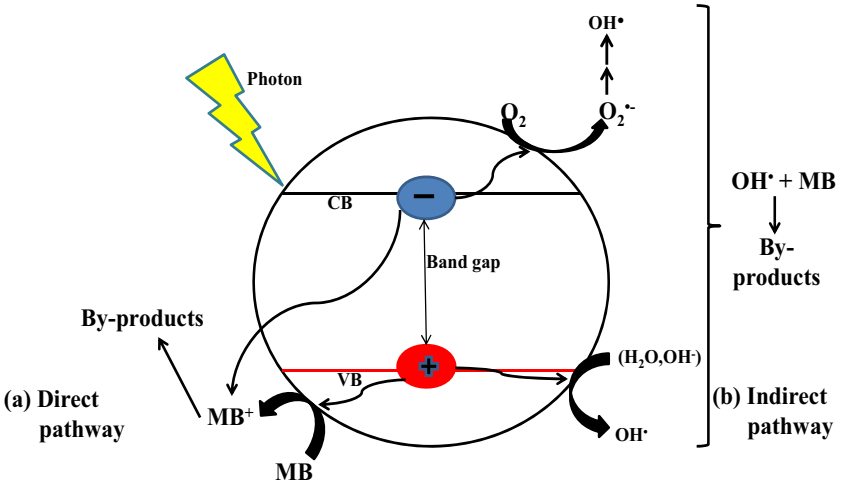

Scheme 2. Proposed mechanism for the photocatalytic decoloration of MB.

scavengers of OH radical and react poorly with holes [43,44]. 4 mL of ethanol was added to the solutions (pH 11 and 7) containing MB and catalyst. Results of this experiment are presented in Fig. 10 and show a decrease in the rate of MB decoloration in the presence of ethanol with the exception of T_1:S_3AA at pH 7. This implies that at pH 11, the direct and indirect mechanisms are responsible for MB decoloration with the prevalence of the direct mechanism. At pH 7 where there should be relatively less electrostatic interaction between the catalysts and MB, commercial TiO_2 exhibited a very low percentage decoloration in the presence of ethanol, meaning the most dominant decoloration mechanism is the indirect. T_1:S_3AA exhibited relatively higher percentage decoloration of MB in the presence of ethanol compared with photodegradation experiment done in the absence of ethanol (Fig. 10a). This result correlates with the percentage of MB adsorbed on the material (Fig. 10b) after equilibrating in the dark, and suggests an enhanced adsorption of MB by T_1:S_3AA in the presence of ethanol. This means in neutral MB solution, the predominant mechanism of decoloration exhibited by T_1:S_3AA is via the direct route.

4. Conclusions

Polycrystalline mesoporous TiO_2 existing in the anatase phase was synthesized with different concentrations of Pluronic F127. All as-prepared TiO_2 exhibited a relatively higher surface area than the commercial TiO_2 (Degussa P25). The study also showed the effect of surfactant concentration on the formation of active species needed for the oxidation of the model dye. An increased formation rate of OH radical was observed as the concentration of surfactant increased. All as-prepared TiO_2 except T_1:S_1, showed better photocatalytic activity than the commercial TiO_2 under 32 W daylight CFL. T_1:S_3AA synthesized with the highest concentration of surfactant and calcined in air and argon, among other materials generated highest concentration of OH radical and showed better photocatlytic activity. The proposed mechanism for the characteristic photocatalytic behavior of the as-prepared TiO_2 is through the direct and the indirect route unlike the commercial TiO_2 which is more of the indirect mechanism.

Acknowledgments

The authors appreciates the School of Chemistry and Physics, University of KwaZulu-Natal, Westville Campus, Durban; and iThemba LABS, Materials Research Department, South Africa for access to the facilities used for the research. We also thank Professor Orde Munro of the School of Chemistry and Physics, University of KwaZulu-Natal, Pietermaritzburg Campus for assisting with the ESR experiment.

References

[1] M.A. Rauf, S.S. Ashraf, Chem. Eng. J. 151 (2009) 10–18.
[2] A.E.H. Machado, J.A. de Miranda, R.F. de Freitas, E. Duarte, L.F. Ferreira, Y.D.T. Albuquerque, R. Ruggiero, C. Sattler, L. de Oliveira, J. Photochem. Photobiol. A-Chem. 155 (2003) 231–241.
[3] C.G. da Silva, J.L. Faria, J. Photochem. Photobiol. A-Chem. 155 (2003) 133–143.
[4] M.N. Chong, B. Jin, C.W.K. Chow, C. Saint, Water Res. 44 (2010) 2997–3027.
[5] A. Sirisuk, E. Klansorn, P. Praserthdam, Catal. Commun. 9 (2008) 1810–1814.
[6] D.P. Macwan, P.N. Dave, S. Chaturvedi, J. Mater. Sci. 46 (2011) 3669–3686.
[7] E.O. Oseghe, P.G. Ndungu, S.B. Jonnalagadda, Environ. Sci. Pollut. Res. 22 (2015) 211–222.
[8] B. Tryba, M. Toyoda, A.W. Morawski, R. Nonaka, M. Inagaki, Appl. Catal. B-Environ. 71 (2007) 163–168.
[9] R. Jiang, H.Y. Zhu, H.H. Chen, J. Yao, Y.Q. Fu, Z.Y. Zhang, Y.M. Xu, Appl. Surf. Sci. 319 (2014) 189–196.
[10] G. Yang, T. Wang, B. Yang, Z. Yan, S. Ding, T. Xiao, Appl. Surf. Sci. 287 (2013) 135–142.
[11] V.D. Binas, K. Sambani, T. Maggos, A. Katsanaki, G. Kiriakidis, Appl. Catal. B-Environ. 113 (2012) 79–86.
[12] M. Li, X. Li, G. Jiang, G. He, Ceramics Int. 41 (2015) 5749–5757.
[13] E. Beyers, P. Cool, E.F. Vansant, J. Phys. Chem. B 109 (2005) 10081–10086.
[14] D.S. Kim, J.-D. Jeon, K.-H. Shin, Micropor. Mesopor. Mater. 181 (2013) 61–67.
[15] Q. Xiao, L. Ouyang, Chem. Eng. J. 148 (2009) 248–253.
[16] N. Aman, P.K. Satapathy, T. Mishra, M. Mahato, N.N. Das, Mater. Res. Bull. 47 (2012) 179–183.
[17] M. Hojamberdiev, R.M. Prasad, K. Morita, M.A. Schiavon, R. Riedel, Micropor. Mesopor. Mater. 151 (2012) 330–338.
[18] A.I. Maldonado-Valdivia, E.G. Galindo, M.J. Ariza, M.J. Garcia-Salinas, Sol. Energy 91 (2013) 263–272.
[19] L. Hongjun, Z. Zang, X. Tang, Opt. Mater. Express 4 (2014) 1762–1769.
[20] H. Yu, S. Ouyang, S. Yan, Z. Li, T. Yu, Z. Zou, J. Mater. Chem. 21 (2011) 11347–11351.
[21] Z. Zang, X. Tang, J. Alloys Compd. 619 (2015) 98–101.
[22] N.A. Ramos-Delgado, M.A. Gracia-Pinilla, L. Maya-Trevino, L. Hinojosa-Reyes, J.L. Guzman-Mar, A. Hernandez-Ramirez, J. Hazard. Mater. 263 (2013) 36–44.
[23] V. Kiran, S. Sampath, Nanoscale 5 (2013) 10646–10652.
[24] K.S.W. Sing, D.H. Everett, R.A.W. Haul, L. Moscou, R.A. Pierotti, J. Rouquerol, T. Siemieniewska, Pure Appl. Chem. 57 (1985) 603–619.
[25] S.A.K. Leghari, S. Sajjad, F. Chen, J. Zhang, Chem. Eng. J. 166 (2011) 906–915.
[26] V. Meynen, P. Cool, E.F. Vansant, Micropor. Mesopor. Mater. 125 (2009) 170–223.
[27] D.S. Kim, S.-Y. Kwak, Appl. Catal. A-Gen. 323 (2007) 110–118.
[28] Y. Wan, D. Zhao, Chem. Rev. 107 (2007) 2821–2860.
[29] N.M. Dimitrijevic, B.K. Vijayan, O.G. Poluektov, T. Rajh, K.A. Gray, H. He, P. Zapol, J. Am. Chem. Soc. 133 (2011) 3964–3971.
[30] Y. Nakaoka, Y. Nosaka, J. Photochem. Photobiol. A-Chem. 110 (1997) 299–305.
[31] A.D. Daisy, N. Rajasekaran, S.J. Das, R. Jagannathan, Chem. Phys. Lett. 548 (2012) 34–39.
[32] I.R. Macdonald, S. Rhydderch, E. Holt, N. Grant, J.M.D. Storey, R.F. Howe, Catal. Today 182 (2012) 39–45.
[33] B. Kasprzyk-Hordern, M. Ziolek, J. Nawrocki, Appl. Catal. B-Environ. 46 (2003) 639–669.
[34] Q. Xiang, J. Yu, P.K. Wong, J. Colloid Interface Sci. 357 (2011) 163–167.
[35] J. Yu, W. Wang, B. Cheng, B.-L. Su, J. Phys. Chem. C 113 (2009) 6743–6750.
[36] Z.-D. Meng, L. Zhu, J.-G. Choi, C.-Y. Park, W.-C. Oh, Nanoscale Res. Lett. 6 (2011).
[37] M.A. Rauf, M.A. Meetani, S. Hisaindee, Desalination 276 (2011) 13–27.
[38] D. Friedmann, C. Mendive, D. Bahnemann, Appl. Catal. B-Environ. 99 (2010) 398–406.
[39] I.K. Konstantinou, T.A. Albanis, Appl. Catal. B-Environ. 49 (2004) 1–14.
[40] R. Rosal, A. Rodriguez, M.S. Gonzalo, E. Garcia-Calvo, Appl. Catal. B-Environ. 84 (2008) 48–57.
[41] B. Abramovic, D. Sojic, V. Despotovic, D. Vione, M. Pazzi, J. Csanadi, Appl. Catal. B-Environ. 105 (2011) 191–198.
[42] M.I. Litter, Appl. Catal. B-Environ. 23 (1999) 89–114.
[43] N. Daneshvar, D. Salari, A.R. Khataee, J. Photochem. Photobiol. A-Chem. 162 (2004) 317–322.
[44] M.E. Carlotti, E. Ugazio, L. Gastaldi, S. Sapino, D. Vione, I. Fenoglio, B. Fubini, J. Photochem. Photobiol. B-Biol. 96 (2009) 130–135.